FULL PAPER

DOI: 10.1002/chem.200700739

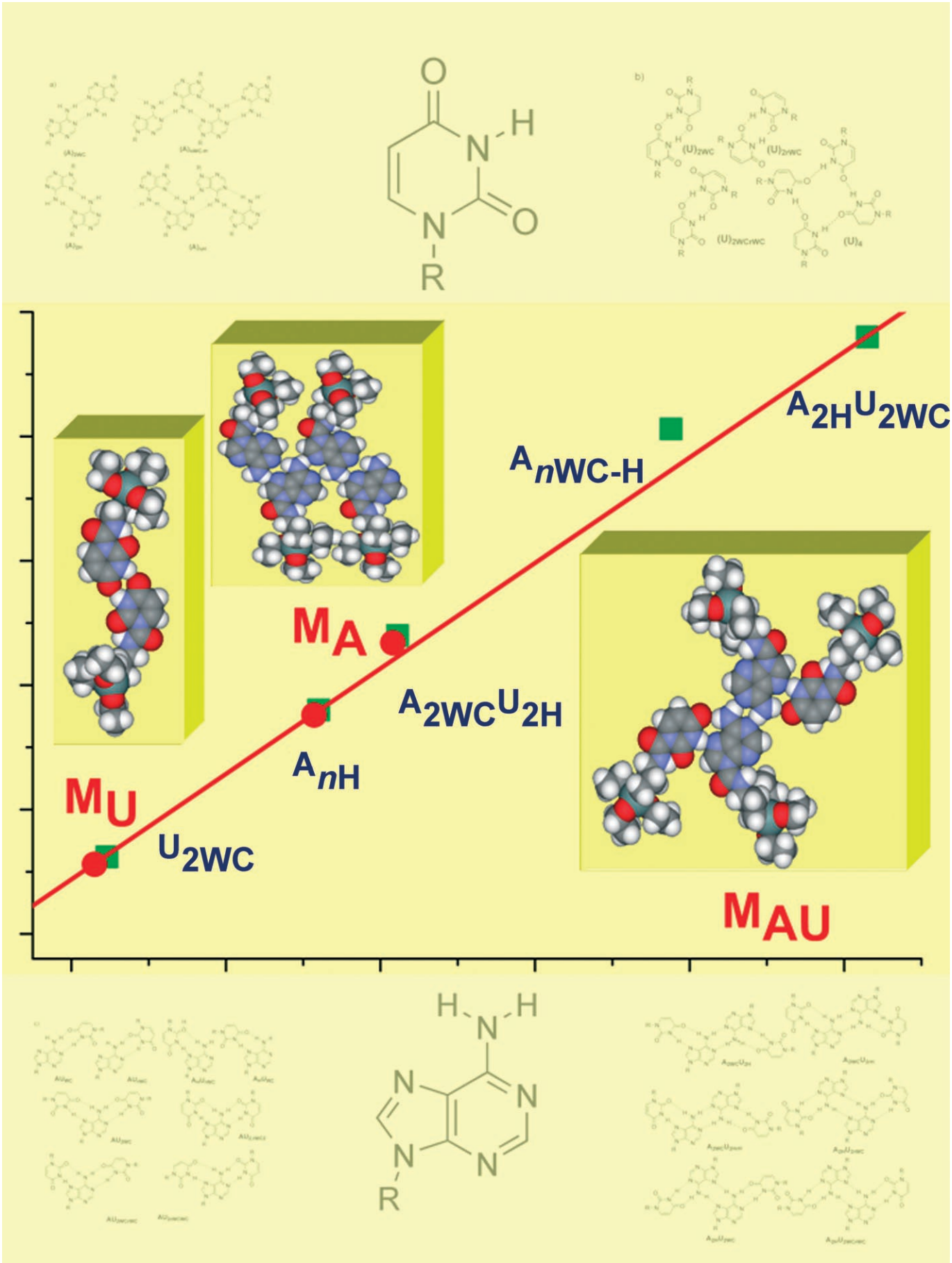

Constitutional Self-Organization of Adenine–Uracil-Derived Hybrid Materials

Carole Arnal-Hérault,[a] Mihai Barboiu,*[a] Andreea Pasc,[a, b] Mathieu Michau,[a] Pascal Perriat,[c] and Arie van der Lee[a]

Abstract: The alkoxysilane nucleobase adenine (**A**) and uracil (**U**) precursors described in this paper generate in solution a complex library of hydrogen-bonded aggregates, which can be expressed in the solid state as discrete higher oligomers. The different interconverting outputs that nucleobases may form by oligomerization define a dynamic polyfunctional diversity that may be "extracted selectively" in solid state by sol–gel transcription, under the intrinsic stability of the system. After the sol–gel process, unique constitutional preference for specific geometries in hybrid materials is consistent with a preferential arrangement of nucleobase systems, favoring the self-assembly by the Hoogsteen geometry. FTIR and NMR spectroscopy and X-ray powder diffraction experiments demonstrate the formation of self-organized hybrid supramolecular materials. Electron microscopy reveals the micrometric platelike morphology of the hybrid materials. The $\mathbf{M_{A-U}}$ hybrid material is nanostructured in ordered circular domains of 5 nm in diameter of alternative light and dark rows with an one-dimensional periodicity of 3.5 Å.

Keywords: adenine · hydrogen bonds · organic–inorganic hybrid composites · self-assembly · sol–gel processes · uracil

Introduction

Nanosized supramolecular materials have received increasing attention over the last two decades.[1–7] Supramolecular synthesis provides a powerful tool for the non-covalent generation of such functional supramolecular architectures.[1] Supramolecular polymers offer solutions for material molding at the macroscopic level, but their manipulation at the molecular (supramolecular) and nanoscopic levels is still difficult to controll.[1,2]

Such polymers may be divided into two partially overlapping classes: 1) supramolecular polymers formed by spontaneous polyassociation of a large number of monomers into the large polymeric architectures through non-covalent interactions (hydrogen bonding,[1d,e,2] van der Waals,[1f,g] metal-ion coordination,[1h] etc.) or reversible covalent bonds;[1d] 2) supramacromolecular polymers resulting from intermolecular self-organization of molecular components during a polymerization process or by molecular recognition of polymeric backbones bearing self-assembling functional groups (Figure 1a).[1c,3–8]

Many groups including our own, have found new methods for the elaboration of such self-organized nanomaterials by sol–gel process. Shinkai and co-workers made an important advancement and they provided useful insights in this field by using organogels acting as robust macrotemplates during sol–gel processes on supramolecular surfaces.[4] Silsesquioxane-based precursors, in which the functional organic and siloxane inorganic groups are covalently linked, are extensively employed for the controlled generation of self-organized materials. Rigid aromatic molecules developed by Corriu et al.,[5] urea hydrogen-bonding ribbons,[6–8] or heterogeneous catalysis[6d,7c] described by Moreau et al.[6] or by our

[a] Dr. C. Arnal-Hérault, Dr. M. Barboiu, Dr. A. Pasc, M. Michau, Dr. A. van der Lee
Adaptative Supramolecular Nanosystems Group
Institut Européen des Membranes -ENSCM/UM2/CNRS 5635
IEM/UM2, CC 047, Place Eugène Bataillon
34095 Montpellier Cedex 5 (France)
Fax: (+33) 467-14-91-19
E-mail: barboiu@iemm.univ-montp2.fr

[b] Dr. A. Pasc
Present address: Université Henri Poincaré-Nancy I
UMR SRSMC 7565, B.P. 239
54506 Vandeouvre-les-Nancy Cedex (France)

[c] Dr. P. Perriat
MATEIS (GEMPPM) UMR-CNRS 5510, INSA de Lyon
Batiment, Blaise Pascal, 7 Avenue Jean capelle
69621 Villeurbane Cedex (France)

Supporting information for this article is available on the WWW under http://www.chemeurj.org/ or from the author.

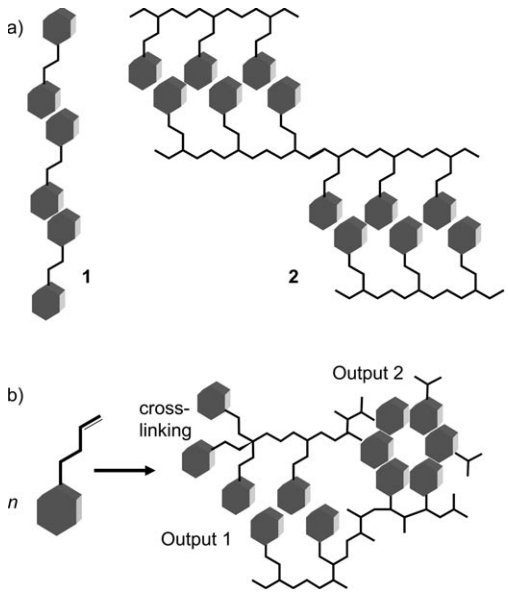

Figure 1. a) Supramolecular (**1**) and supramacromolecular (**2**) polymers resulting from intermolecular and intermacromolecular self-organization; b) cross-linking and multiple output generation after the polymerization of monomers in supramacromolecular polymorphs.

group[7] are used to transcribe a supramolecular self-organization in a siloxane matrix by a sol–gel process.

Despite such impressive progress, considerable challenges still lie ahead and the more significant one is the "dynamic marriage" between supramolecular self-assembly and the polymerization process, which might communicate kinetically and sterochemically to converge to supramolecular self-organization and functions in hybrid materials. The weak supramolecular interactions (hydrogen bonds, coordination, or van der Waals interactions, etc.) positioning the molecular components to give the supramolecular architectures are typically less robust than the cross-linked covalent bonds formed in a specific polymerization process. Accordingly, the sole solution to overcome these difficulties is to improve the binding (association) efficiency of molecular components generating supramolecular assemblies. At least in theory, an increased number of interactions between molecular components and the right selection of the solvent might improve the stability of the templating supramolecular systems communicating with the inorganic siloxane network.

Among these systems, nucleobases,[2a,8] nucleosides,[9] and DNA[10] are known to have a high ability to form directionally controlled multiple intermolecular hydrogen bonding of complementary nature, C–H···O, hydrophobic, and stacking interactions. Their remarkable self-association properties, through Watson–Crick and Hoogsteen pairing, play a critical role in the stabilization of higer order RNA haipirins loops, double or triple helix DNA, and G-quartets or G-quadruplexes.[8,9] During the last decades several studies have reported the preparation of discrete supramolecular assemblies,[8] synthetic polymers,[2] and hybrid materials[6e,10] that contain nucleobases or nucleic acids as side groups or at the end of the chains. Very recently, we reported on a long-range amplification of the G-quadruplex supramolecular chirality into hybrid organic-inorganic twisted nanorods followed by the transcription into inorganic silica microsprings.[7e]

Even though the Watson–Crick (WC) base-pairing is prevalent in natural systems, other hydrogen-bonding motifs are present in natural and artificial systems: reverse Watson–Crick (rWC), Hoogsteen (H), reverse Hoogsteen (rH), wobble (Wo) or reverse wobble (rWo).[8] The adenine–uracil interaction, which involves two hydrogen bonds ($K_a \cong 10^2\,\text{M}^{-1}/\text{CDCl}_3$), is weak and nonspecific with respect that of guanine–cytosine, which involves three hydrogen bonds ($K_a \cong 10^3$–$10^5\,\text{M}^{-1}/\text{CDCl}_3$).[8] Homo- and heteropairing of adenine and uracil derivatives, resulting in the formation of interconverting dimers, trimers, and oligomers by the combination of hydrogen-bond pairing, appear inadequate to function in any predefined recognition scheme. Amazingly, a very diverse set of interconverting supramolecular entities (oligomers) may be generated by using only these two nucleobases (see Scheme 1S in the Supporting Information).

In this paper we report the use of adenine and uracil building blocks as molecular precursor to conceive hybrid materials at nanometric scale. Our efforts involve the synthesis and the self-assembly of adeninesiloxane (**A**) and uracilsiloxane (**U**) monomers in hydrogen-bonded supramolecular hybrid architectures. The main strategy is the generation of a dynamic pool of oligomeric ribbon-type or cyclic supramolecular architectures exchanging in solution; these structure are subsequently fixed in a hybrid organic–inorganic material by using a sol–gel transcription process.

Results and Discussions

Synthesis of molecular precursors A and U: 3-Triethoxypropylisocyanate was treated with the corresponding adenine or uracil nucleobase (DMSO, RT, 12 h) to afford the N^9-(3-triethoxysilylpropyl)adeninecarboxamide (**A**; 40%) and N^1-(3-triethoxysilylpropyl)uracil carboxamide (**U**; 50%) precursors, respectively, as white powders (Scheme 1). The grafting of the triethoxysilanepropylcarboxamide (TEPSCA) groups on N^9- (**A**) and N^1-positions (**U**) of the nucleobases limits the hydrogen-bond pairing for these molecules to Watson–Crick and Hoogsteen interactions.

Synthesis of $\mathbf{M_A}$, $\mathbf{M_U}$, and $\mathbf{M_{A-U}}$ hybrid materials: the generation of hybrid materials $\mathbf{M_A}$, $\mathbf{M_U}$, and $\mathbf{M_{A-U}}$ can be achieved using mild sol–gel conditions. In a typical procedure, deionized water (6 equiv) and benzylamine (3 equiv) as a catalyst were added to 2×10^{-2} M solutions of precursors **A**, **U**, or to an equimolar mixture of **A**:**U** (1:1, mol/mol) in acetone. The mixture was kept at room temperature under static conditions for 15 days. The solvent was then evaporated at yielding the hybrid materials $\mathbf{M_A}$, $\mathbf{M_U}$, and $\mathbf{M_{A-U}}$ as the white powders.

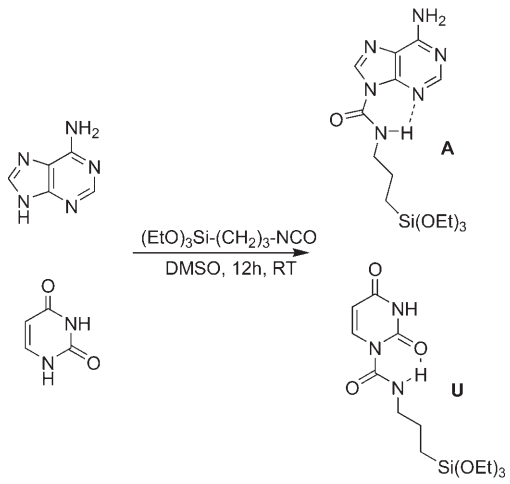

Scheme 1. Synthesis of N^9-(3-triethoxysilylpropyl)adeninecarboxamide (**A**) and N^1-(3-triethoxysilylpropyl)uracilcarboxamide (**U**) precursors.

The precursors **A** and **U** as well as the resulting $\mathbf{M_A}$, $\mathbf{M_U}$, and $\mathbf{M_{A-U}}$ hybrid materials were characterized by FTIR and ^{29}Si NMR-MAS spectroscopy, X-ray powder diffraction (XPRD), scanning electronic microscopy (SEM) and transmission electronic microscopy (TEM).

FTIR and NMR spectroscopic analysis of the hybrid materials indicates the formation of a hybrid supramolecular network. FTIR spectra of hybrid materials $\mathbf{M_A}$, $\mathbf{M_U}$, and $\mathbf{M_{A-U}}$ show broad vibrations at 990–1150 cm^{-1} ($\nu_{Si\text{-}O\text{-}Si}$) instead of the vibrations at 950, 1075, and 1100 cm^{-1} ($\nu_{Si\text{-}OEt}$) initially observed for the molecular precursors **A** and **U**. Evidence for the **A**···**U** hydrogen bonding was obtained from the vibration shifts of the −C=O bonds, detected after hydrolysis–condensation reactions: $\nu_{C=O(A)}$ = 1725–1717, $\nu_{C=O(U)}$ = 1742–1731, and $\nu_{C=O(U)}$ = 1689–1647 cm^{-1} (Supporting Information). ^{29}Si MAS NMR spectroscopic experiments confirm the presence of highly condensed phases within hybrid materials $\mathbf{M_A}$, $\mathbf{M_U}$, and $\mathbf{M_{A-U}}$ (80–85 %), with only a low amount of T1 [C-Si(OSi)$(OH)_2$] (10–14 %) units and containing mainly cross-linked T2 [C-Si$(OSi)_2$ (OH)] (27–29 %) and T3 [C-Si$(OSi)_3$] (54–62 %) units, leading to a predominantly three-dimensional arrangement.

X ray powder diffraction and computational studies: Further insights in the solid-state self-organization of the precursors **A** and **U** and the hybrid materials $\mathbf{M_A}$, $\mathbf{M_U}$, and $\mathbf{M_{A-U}}$ were obtained by X-ray powder diffraction (XPRD). Figure 2 shows that well-defined long-range order is present in the precursors, but also in the hybrid materials after the sol–gel step, albeit that seen in latter is less pronounced than in the precursor materials: there are fewer well-defined peaks present than for the precursor and the average peak width increases, indicating smaller domains in which coherent scattering occurs.

To elucidate the self-organization patterns of the materials, ab initio structure determinations were attempted from the powder data, but they proved to be unsuccessful at this time; this was due to the presence of more than one phase (vide infra), which inevitably causes severe peak overlap and so proper indexing of the peaks was not possible.

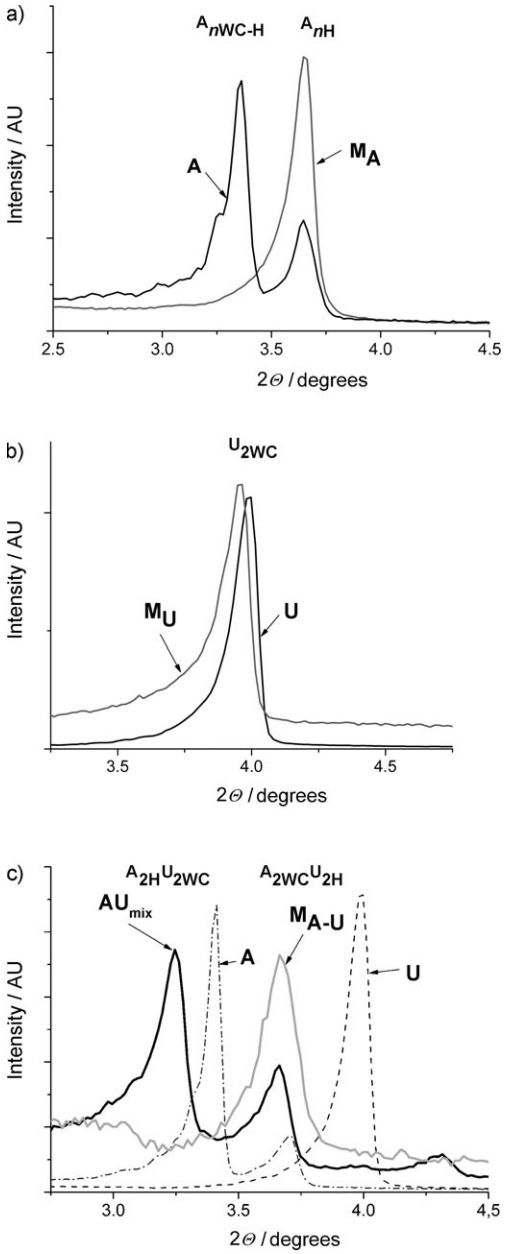

Figure 2. XRPD patterns of a) precursor **A** and hybrid material $\mathbf{M_A}$, b) precursor **U** and hybrid material $\mathbf{M_U}$, and c) a 1:1 mixture $\mathbf{AU_{mix}}$ of **A**:**U** precursors and hybrid material $\mathbf{M_{A-U}}$.

For this reason another approach was chosen to deduce structural information from the diffractograms. To find out which geometry corresponds to which peak, the molecular geometries of **A** and **U** were optimized by means of the Dreiding force field (see the Supporting Information for details). The calculated electronic energies show the intramolecular hydrogen-bonded structures **A** and **U** are favored over the non-hydrogen-bonded ones by 1.1 and 1.4 kcal mol^{-1}, respectively. Moreover, the TEPSCA moiety

is directionally fixed by intramolecular hydrogen bonding, avoiding specific disorders in the structure of the hybrid material (Scheme 2 and Figure 1S in the Supporting Information).

The **A** and **U** precursors generate self-organized superstructures based on two encoded features: 1) they contain a nucleobase moiety that can form ribbon-like oligomers by the combination of hydrogen-bond pairing; 2) the nucleobase moiety is covalently bonded to TEPSCA groups that hydrophobically pack in alternative layers and that can transcribe their self-organized superstructures into solid hybrid materials by sol–gel process. Based on this structural information and on the crystal structures of similar alkylnucleobase derivatives,[11] the relative arrangement of molecules of **A** and **U** in powders and in the $\mathbf{M_A}$, $\mathbf{M_U}$, and $\mathbf{M_{A-U}}$ hybrid materials is probably similar to previously reported crown ether type[7c,d] and ureidoarene[7e] superstructures. As shown in Figure 3a, the postulated model of self-organization is that of parallel hydrogen-bonded nucleobase aggregates and hydrophobic TEPSCA layers which are alternatively stratified and present a tight contact. A characteristic found in all XPRD diffractograms of the precursors **A** and **U** and the hybrid materials $\mathbf{M_A}$, $\mathbf{M_U}$, and $\mathbf{M_{A-U}}$ is the first diffraction peak at *d* spacings between 23.6 and 27.1 Å. (Table 1, Figure 2). It was postulated that this spacing represents the interplanar distance between two Si atoms (d_{Si-Si}, Figure 3b) by using a linear geometry for the propyl substituents. Silicon is the most electron-rich element in the precursors and hybrid materials, so it can be expected that

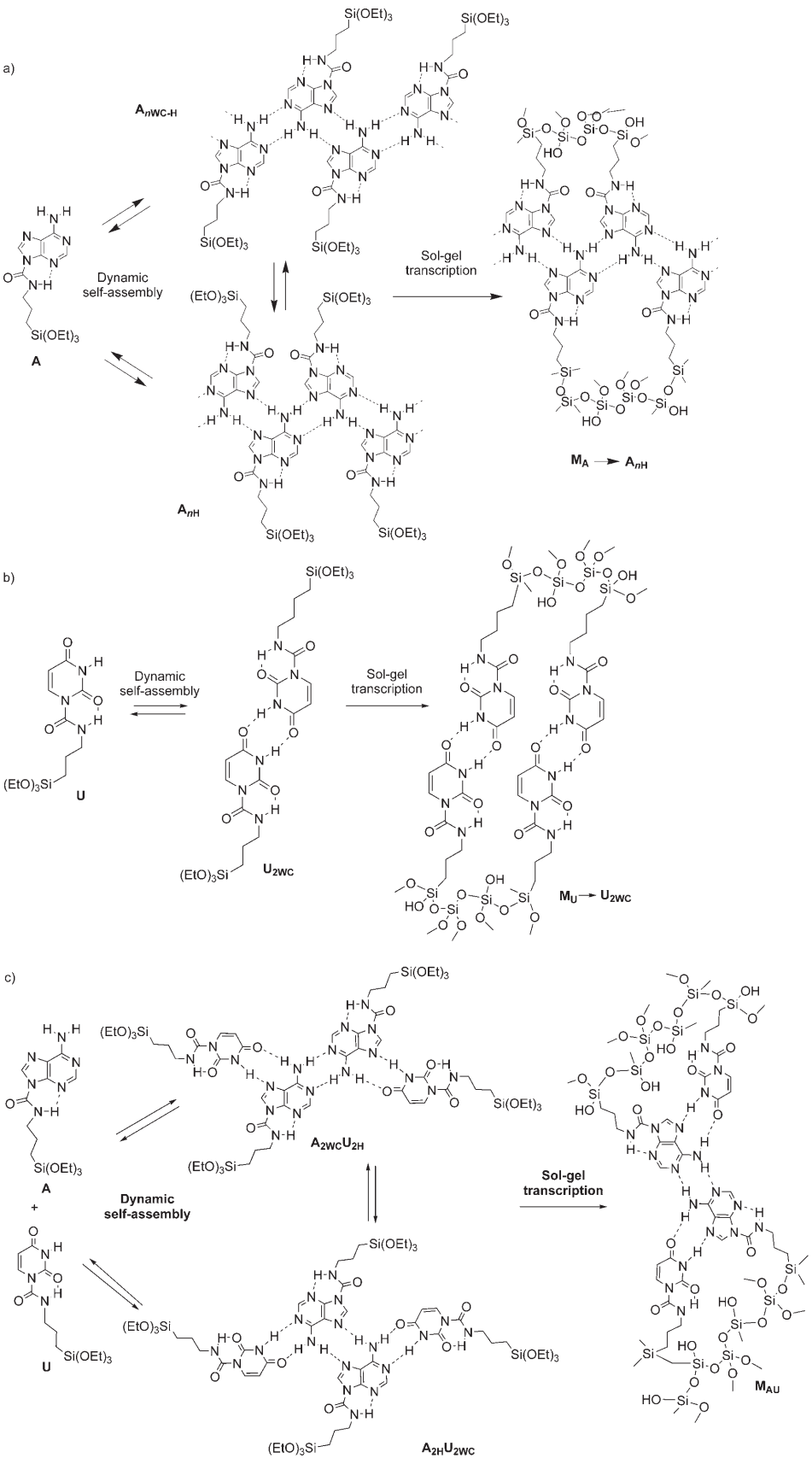

Scheme 2. Dynamic self-assembly in solution and sol–gel transcription of a) precursor A, b) precursor, U and c) a 1:1 mixture of precursors A:U.

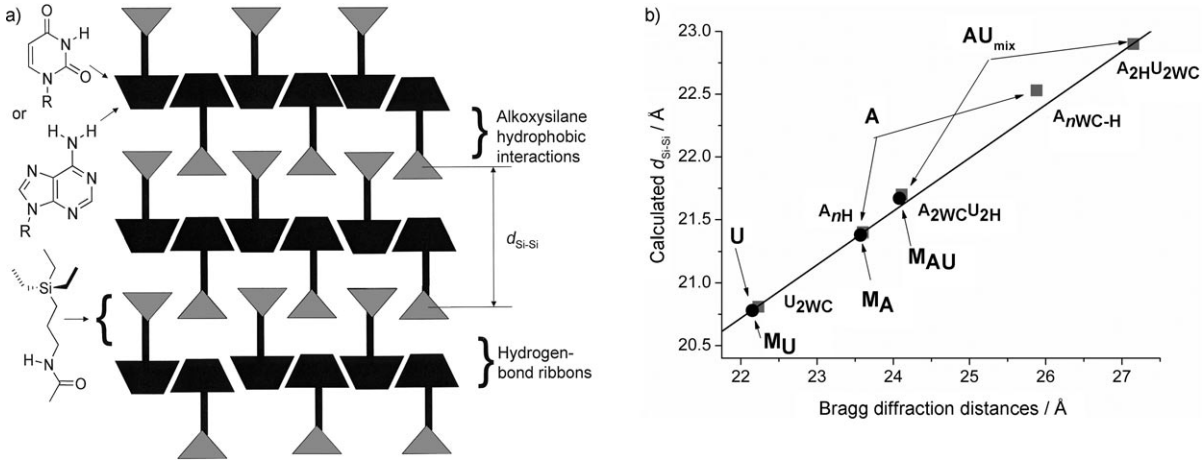

Figure 3. a) Postulated model of self-organization of parallel hydrogen-bonded nucleobase aggregates and hydrophobic propyltriethoxysilane layers; b) interplanar d_{Si-Si} distances calculated from the geometry of minimized structures versus experimental interplanar Bragg diffraction distances (the straight line is just a guide to the eye). The grey squares correspond to the unpolymerized powders of precursors **A**, **U**, and their 1:1 mixture $\mathbf{AU_{mix}}$, while black circles correspond to hybrid materials $\mathbf{M_A}$, $\mathbf{M_U}$, and $\mathbf{M_{A-U}}$.

Table 1. The corresponding Bragg peaks and distances calculated from small angle diffractograms of precursors **A**, **U**, and the 1:1 mixture of **A**:**U** ($\mathbf{AU_{mix}}$), and hybrid materials $\mathbf{M_A}$, $\mathbf{M_U}$, and $\mathbf{M_{A-U}}$.

Precursors and hybrid materials	Bragg diffraction peaks [°]	Bragg diffraction distances [Å]
A	3.41, 3.74	25.9, 23.6
U	3.97	22.2
$\mathbf{AU_{mix}}$	3.25, 3.66	27.1, 24.1
$\mathbf{M_A}$	3.74	23.6
$\mathbf{M_U}$	3.95	22.1
$\mathbf{M_{A-U}}$	3.67	24.1

the strongest peaks in the diffractograms are due to planes containing a relatively high density of Si atoms. These minimized molecular structures were then paired so as to produce the Watson–Crick, reverse Watson–Crick, Hoogsteen, and reverse Hoogsteen geometries by using the hydrogen-bonding distances described in the crystal structures of adenine or 9-methyladenine,[11] uracil or 1-methyluracil,[12] and their adenine–uracil adducts.[13] After optimizing these base-pairs or quartets, the d_{Si-Si} spacing was determined (Table 2, Figure 3S in the Supporting Information) and found to be in perfect linear correlation with the distances corresponding to the first intense diffraction peaks observed in the XRPD patterns (Table 1, Figure 2). Moreover, these distances are very well correlated with the carbon–carbon distances d_{C1-C1} observed in three-dimensional RNA X-ray structures (Figure 4S, in the Supporting Information).

Table 2. Calculated interplanar d_{Si-Si} distances from minimized structures.

Nucleobase oligomer[a]	Calculated d_{Si-Si} [Å]	Nucleobase oligomer[a]	Calculated d_{Si-Si} [Å]
$\mathbf{A_{nWC-H}}$	22.5	$\mathbf{U_{2WC}}$	20.8
$\mathbf{A_{nH}}$	21.4	$\mathbf{U_{2rWC}}$	15.5
$\mathbf{A_{2WC}U_{2H}}$	21.7	$\mathbf{U_4}$	24.6
$\mathbf{A_{2H}U_{2WC}}$	22.9		

[a] For details see Scheme 1S or Figure 3S in the Supporting Information; the self-assembling of $\mathbf{U_{2WCrWC}}$, $\mathbf{A_{2WC}U_{2HrH}}$, $\mathbf{A_{2WC}U_{2rH}}$, $\mathbf{A_{2H}U_{2WCrWC}}$, and $\mathbf{A_{2H}U_{2rWC}}$ oligomers shown in Scheme 1S are stereochemically hindered by the bulky blocking alkoxysilanecarboxamide groups of two neighboring nucleobase motifs.

As a general rule, as shown by the differences between the values of interplanar Bragg diffraction distances, the condensation process between the ethoxysilane groups during the sol–gel process results in the formation of the more compact hybrid materials $\mathbf{M_A}$, $\mathbf{M_U}$, and $\mathbf{M_{A-U}}$ relative to the unpolymerized **A**, **U**, and $\mathbf{AU_{mix}}$ powders (Table 1 and Figure 3b).

The small-angle XRPD pattern of the precursor **A**, recrystallized in ethanol or acetonitrile, has two well-resolved Bragg diffraction peaks at $2\theta = 3.41°$ ($d = 25.9$ Å) and $2\theta = 3.74°$ ($d = 23.6$ Å) corresponding to two crystallographycally distinct phases: $\mathbf{A_{nWC-H}}$ and $\mathbf{A_{nH}}$ oligomers (Figure 2a). A freshly synthesized solid sample of **A** is predominantly crystallized as Watson–Crick/Hoogsteen $\mathbf{A_{nWC-H}}$ oligomer. A second non-predominant polymorph of the all-Hoogsteen $\mathbf{A_{nH}}$ oligomers are present in powder as a result of breaking of Watson–Crick hydrogen bonds and creation of the new Hoogsteen hydrogen bonds. The small-angle XRPD pattern of hybrid material $\mathbf{M_A}$ presents a unique well-resolved Bragg diffraction peak at $2\theta = 3.74°$ ($d = 23.6$ Å; Figure 2a), corresponding to a crystallographically distinct and unique phase $\mathbf{A_{nH}}$.

The two-dimensional molecular packing of the adenine absorbed on graphite has been studied by STM[11a] and AFM;[11a] it crystallizes in two-dimensional supramolecular tapes through the formation of Hoogsteen N^6–H···N^9 hydrogen bonds. Similarly, 9-methyladenine[11c,d] and 9-ethyladenine[11e] crystallize through the formation of unique Hoogsteen hydrogen bonds, in two-dimensional layers. These layers, which are alternatively stratified, exhibit two types of interfaces: one surface contact due to the π–π stacking of adenine tapes and another resulting from hydrophobic interactions of alkyl groups, which form in van der

Waals interactions. Similarly, the structures of the $\mathbf{A}_n$ oligomers are most likely dictated by hydrophobic interactions between the grafted ethoxysilanepropylcarboxamide groups (Figure 3a). In a freshly prepared sample of **A**, the solvent logged between hydrophobic groups favors the extended $\mathbf{A}_{n\mathbf{WC-H}}$ oligomers. The condensation reaction between the ethoxysilane groups during the sol–gel process favors the more compact $\mathbf{A}_{n\mathbf{H}}$ oligomers in which the hydrophobic groups are interlocked, stabilizing thus the interaction between adenine Hoogsteen hydrogen-bonded layers.

The small-angle XRPD patterns of the precursor **U** and of the hybrid material $\mathbf{M_U}$ have one Bragg diffraction peak each at $2\theta = 3.97°$ ($d = 22.2$ Å) and $2\theta = 3.95°$ ($d = 22.1$ Å) (Figure 2b), respectively, corresponding to a characteristic Watson–Crick $\mathbf{U_{2WC}}$ dimer ($d_{Si-Si} = 20.8$ Å) (Figure 3). The two other possible structures, the dimer $\mathbf{U_{2rWC}}$ ($d_{Si-Si} = 15.5$ Å) and the quartet $\mathbf{U_4}$ ($d_{Si-Si} = 24.6$ Å) do not correlate with the experimental data.

A freshly evaporated solid sample of an equimolecular mixture of **A** and **U** in acetone leads to two Bragg diffraction peaks in the diffraction pattern at $2\theta = 3.66°$ ($d = 24.1$ Å) and $2\theta = 3.25°$ ($d = 27.1$ Å), corresponding to the oligomers $\mathbf{A_{2WC}U_{2H}}$ and $\mathbf{A_{2H}U_{2WC}}$, respectively. The small-angle XRPD pattern of the hybrid material $\mathbf{M_{A-U}}$ has a Bragg diffraction peak at $2\theta = 3.67°$ ($d = 24.1$ Å), corresponding to a characteristic interplanar $d_{Si-Si} = 21.7$ Å distance of the Watson–Crick $\mathbf{A_{2WC}U_{2H}}$ oligomer (Figure 3). Amazingly, the unique structure of the resulting hybrid material $\mathbf{M_{A-U}}$ is consistent with the formation of Hoogsteen base pairs between uracil and adenine and Watson–Crick base pairs between two adenine molecules. Early contributions by Etter,[13a] Diederich,[13b] and others have recently been confirmed through calculations performed by Zimmermann;[13c] they indicate an almost exclusive preference for Hoogsteen binding within 1:1 base-pairing complexes between alkyladenine and alkylthymine derivatives.[14] Although many have recognized that in the solid state the uracil or thymine moieties preferentially bind adenine through Hoogsteen binding, here the $\mathbf{A_{2WC}U_{2H}}$ oligomer is quantitatively amplified from a dynamic pool of oligomers in solution through sol–gel transcription.

The wide-angle XRPD patterns of the hybrid materials $\mathbf{M_A}$, $\mathbf{M_U}$, and $\mathbf{M_{A-U}}$ have many well-resolved peaks in the range 10–30°, indicating that these hybrid materials have reasonably well ordered structures (Figure 4S, Supporting Information). The Bragg diffraction peak at $2\theta = 24.5°$ ($d = 3.5$ Å) corresponds to a characteristic π–π stacking distance between two planar ribbon-like oligomers.

Electronic microscopy studies: Scanning electron microscopy (SEM) micrographs reveal that the hybrid materials $\mathbf{M_A}$ (Figure 4a) and $\mathbf{M_U}$ (Figure 4a) have a micrometric platelike morphology, while the $\mathbf{M_{A-U}}$ hybrid material (Figure 4c) consists of crystalline nanorods.

Transmission electron microscopy (TEM) experiments of hybrid material $\mathbf{M_{A-U}}$ show that the structure is characterized by a short-range ordered circular domains of 5 nm in diameter. These oriented domains and the semicrystalline nature of the material after the sol–gel process are clearly seen in the Figure 5. The *d* spacings of 3.5 Å are observed between alternate light, inorganic, siloxane layers and dark, organic, hydrogen-bonded nucleobased rows with a periodicity in one direction. The match between the periodicity of parallel sheets and the distances observed in the XPRD experiments ($2\theta = 24.5° \rightarrow d = 3.5$ Å) indicates that the hybrid material $\mathbf{M_{A-U}}$ has a sheet-like superstructure with an interlayer distance corresponding probably to the stacking interactions between nucleobases nano-ribbons (a lateral view in presumed model in Figure 3a).

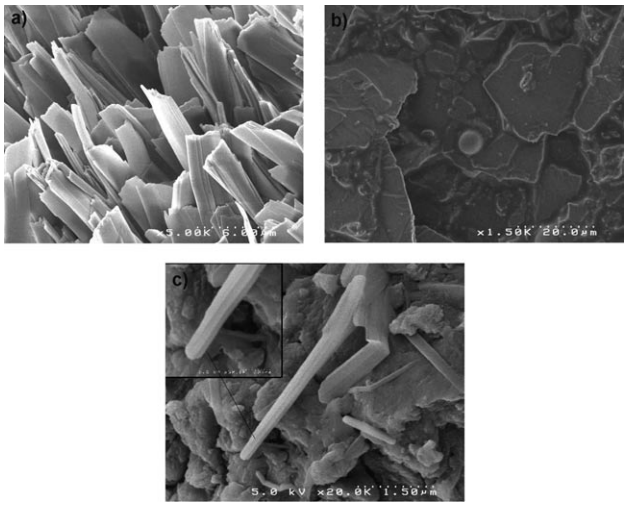

Figure 4. SEM images of a) $\mathbf{M_A}$, b) $\mathbf{M_U}$, and c) $\mathbf{M_{A-U}}$ hybrid materials.

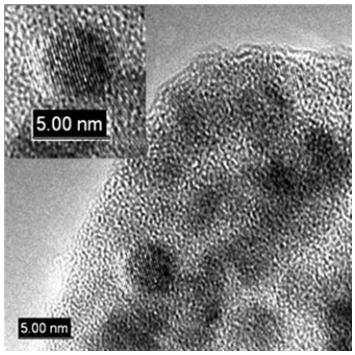

Figure 5. TEM image of the $\mathbf{M_{A-U}}$ hybrid material.

The X-ray structural data and microscopy analysis allow the following conclusions to be drawn.

1) In solution the precursors form different types of hydrogen-bonded aggregates that can be expressed in the solid state as discrete higher unpolymerized oligomers based on different possible hydrogen-bond base pairing: $\mathbf{A}_{n\mathbf{WC-H}}$ and $\mathbf{A}_{n\mathbf{H}}$ for **A**, $\mathbf{U_{2WC}}$ dimer for **U**, and $\mathbf{A_{2WC}U_{2H}}$ and $\mathbf{A_{2H}U_{2WC}}$ for the equimolar mixture $\mathbf{AU_{mix}}$.

2) After the sol–gel process, the constitutional preference for $\mathbf{M_A}\rightarrow\mathbf{A}_{n\mathbf{H}}$ (Scheme 2a) , $\mathbf{M_U}\rightarrow\mathbf{U_{2WC}}$ (Scheme 2b) and $\mathbf{M_{A-U}}\rightarrow\mathbf{A_{2WC}U_{2H}}$ (Scheme 2c) geometries in polymerized hybrid materials is consistent with the natural arrangement of similar systems favoring the self-assembly in an compact Hoogsteen geometry.[13,14].

Conclusion

The above results describe the formation and the interconversion of hydrogen-bond architectures derived from the alkoxysilane adenine (**A**) and uracil (**U**) nucleobase precursors that are subsequently fixed in the hybrid organic-inorganic materials by means of a sol–gel transcription process. Dynamic self-assembly of supramolecular systems, undergoing continous reversible exchange between different self-organized entities, may in principle be connected to kinetically controled sol–gel processes in order to extract and select an amplified supramolecular device under a specific set of experimental conditions. Such a "dynamic marriage" between supramolecular self-assembly and sol–gel polymerization processes that sinergistically might communicate leads to "constitutionally driven hybrid materials".

Nucleobase oligomerization[8] by hydrogen bonding can be an advantageous choice to reinforce the controlled communication between interconnected "dynamic supramolecular" and "fixing siloxane" systems. Moreover, the hydophobic interactions can play an important role in the stabilization of compact packed superstructures, which may be "extracted selectively" under the intrinsic stability of the system or external stimuli by polymerization in the solid state.

The combined features of dynamic constitutional diversity, controlled generation of hybrid materials by self-organization, and potential addressability make processes and species such as those presented here of interest for the development of a supramolecular constitutional approach to nanomaterials through "self-fabrication" toward systems of increasing complexity.

Experimental Section

Materials and methods: Adenine, uracil, and 3-triethoxypropylisocyanate were purchased from Aldrich and used as received. All other reagents were obtained from commercial suppliers and used without further purification. All organic solvents were routinely dried by using sodium sulfate (Na_2SO_4). ^{1}H and ^{13}C NMR spectra were recorded on an ARX 300 MHz Bruker spectrometer in [D_6]DMSO with the use of the residual solvent peak as reference. Solid-state NMR was performed on a Bruker ASX400 spectrometer. Mass spectrometric studies were performed in the positive ion mode on a quadrupole mass spectrometer (Micromass, Platform 2+). Samples were dissolved in acetonitrile and were continuously introduced into the mass spectrometer at a flow rate of 5 mL min^{-1} through a Waters 616HPLC pump. The temperature (60 °C) and the extraction cone voltage (V_c = 30 V) were set to avoid fragmentations. X-ray powder diffraction measurements were performed with $Cu_{K\alpha}$ radiation at 20 °C on a Philips X'Pert diffractometer equipped with an Xcelerator detector. SEM images were obtained with a Hitachi S-4500 apparatus, under a tension of 0.5–30 kV.

Synthesis of N^9-(3-triethoxysilylpropyl)adeninecarboxamide A: 3-(Triethoxysilyl)propylisocyanate (3.7 g, 14.80 mmol) was added to a suspension of adenine (2 g, 14.80 mmol) in DMSO (50 mL). The reaction was stirred for 12 h at room temperature. The reaction mixture was then precipitated in ice water, and the precipitate was filtered and recrystallized from ethanol or acetonitrile to afford compound **A** as white powder (2.26 g, 5.91 mmol; 40 %). ^{1}H NMR ([D_6]DMSO, 300 MHz): δ = 8.94 (s, 1H), 8.53 (s, 1H), 8.37 (s, 1H), 6.15 (s, 2H), 3.84 (q, J = 6.98 Hz; 6H), 3.51 (q, J = 6.62 Hz; 2H), 1.82 (q, J = 7.25 Hz; 2H), 1.24 (t, J = 6.98 Hz; 9H), 0.74 ppm (t, J = 8.4 Hz; 2H); ^{13}C NMR ([D_6]DMSO, 300 MHz): δ = 155.9, 153.1, 149.0, 148.3 139.3, 120.1, 58.5, 42.9, 23.1, 18.3, 7.8 ppm; MS (ESI): m/z (%): 384.2 (100) [**A**+H]$^+$

Synthesis of N^1-(3-triethoxysilylpropyl)uracilcarboxamide (U): Uracil (2 g, 17.84 mmol) was dissolved in DMSO (50 mL) and 3-(triethoxysilyl)-propylisocyanate (4.4 g, 17.84 mmol) was added. The mixture was stirred for 12 h at room temperature, and then poured in to ice water. The precipitate was filtered and recrystallized from hexane to afford compound **U** as white powder (3.21 g, 8.90 mmol; 50 %). ^{1}H NMR ([D_6]DMSO, 300 MHz): δ = 11.74 (s, 1H), 9.12 (s, 1H), 8.19 (d, J = 8.43 Hz; 1H), 5.79 (d, J = 2.12 Hz; 1H), 3.75 (q, J = 6.98 Hz; 6H), 3.25 (q, J = 6.72 Hz; 2H), 1.57 (q, J = 7.80 Hz; 2H), 1.14 (t, J = 6.98 Hz; 9H), 0.58 ppm (t, J = 8.4 Hz; 2H); ^{13}C NMR ([D_6]DMSO, 300 MHz): δ = 162.3, 151.5, 149.7, 139.0, 103.8, 58.5, 43.7, 22.8, 18.3, 7.7 ppm; MS (ESI): m/z (%): 360.6 (100) [**U**+H]$^+$

General procedure for the synthesis of hybrid materials $\mathbf{M_A}$, $\mathbf{M_U}$, and $\mathbf{M_{A-U}}$: In a typical sol–gel experiment the precursors **A** (0.20 g, 0.52 mmol), **U** (0.19 g, 0.52 mmol), or the equimolar mixture of **A** (0.20 g, 0.52 mmol) and **U** (0.19 g, 0.52 mmol) were dissolved in acetone (20 mL). Then deionized water (0.056 g, 3.13 mmol for $\mathbf{M_A}$ or $\mathbf{M_U}$ and 0.11 g, 6.27 mmol for $\mathbf{M_{A-U}}$) and benzylamine (0.055 g, 0.52 mmol for $\mathbf{M_A}$ or $\mathbf{M_U}$ and 0.11 g, 1.05 mmol for $\mathbf{M_{A-U}}$) as a catalyst were added. Samples were kept under static conditions at room temperature for eight days. Then the solvent was then slowly removed at room temperature yielding the hybrid materials $\mathbf{M_A}$, $\mathbf{M_u}$ and $\mathbf{M_{A-U}}$ as white or light yellow powders.

Acknowledgement

This work, conducted as part of the award "Dynamic adaptive materials for separation and sensing Microsystems" (M.B.) made under the European Heads of Research Councils and European Science Foundation EURYI (European Young Investigator) Awards Scheme in 2004, was supported by funds from the Participating Organizations of EURYI and the EC Sixth Framework Program (see www.esf.org/euryi) This research was also supported in part by the CNRS and the University of Montpellier 2.

[1] a) J.-M. Lehn, *Supramolecular Chemistry-Concepts and Perspectives*, VCH, Weinheim, **1995**; b) J.-M. Lehn, *Proc. Natl. Acad. Sci. USA* **2002**, *99*, 4763–4768; c) *Supramolecular Polymers*, 2nd ed. (Ed.: A. Ciferi), CRC, Taylor and Francis, Boca Raton, **2005**; d) J.-M. Lehn, in *Supramolecular Polymers*, 2nd ed. (Ed.: A. Ciferi), CRC, Taylor and Francis, Boca Raton, **2005**, Chapter 1, pp. 3–27; e) J.-M. Lehn, *Chem. Soc. Rev.* **2007**, *36*, 151–160; f) J. J. L. M. Cornelissen, M. Fischer, N. A. J. M. Sommerdijk, R. J. M. Nolte, *Science* **1998**, *280*, 1427–1430; g) H. Engelkamp, S. Middelbeek, R. J. M. Nolte, *Science* **1999**, *284*, 785–788; h) P. R. Andres, U. S. Schubert, *Adv. Mater.* **2004**, *16*, 1043–1068.

[2] a) S. Sivakova, S. T. Rowan, *Chem. Soc. Rev.* **2005**, *34*, 9–21; b) A. Khan, D. M. Haddleton, M. J. Hannon, D. Kukulj, A. Marsh, Macromolecules, **1999**, *32*, 6560–6569; c) J. F. Lutz, A. F. Thunemann, R. Nehring, *J. Polym. Sci. Part A* **2005**, *43*, 4805–4818.

[3] a) C. Sanchez, F. Ribot, *New J. Chem.* **1994**, *18*, 1007–1047; b) C. Sanchez, B. Julian, P. Belleville, M. Popall, *J. Mater. Chem.* **2005**, *15*, 3559–3592; c) *Functional Hybrid Materials* (Eds.: P. Gomez-Romero, C. Sanchez), Wiley-VCH, Weinheim, **2004**.
[4] K. J. C. van Bommel, A. Frigerri, S. Shinkai, *Angew. Chem.* **2003**, *115*, 1010–1030; *Angew. Chem. Int. Ed. Ed. Engl.* **2003**, *42*, 980–999
[5] a) R. J. P. Corriu, *Eur. J. Inorg. Chem.* **2001**, *5*, 1109–1121; b) F. Ben, B. Boury, R. J. P. Corriu, P. Delord, M. Nobili, *Chem. Mater.*, **2002**, *14*, 730–738.
[6] a) J. J. E. Moreau, L. Vellutini, M. Wong Chi Man, C. Bied, J. L. Bantignies, P. Dieudonné, J. L. Sauvajol, *J. Am. Chem. Soc.* **2001**, *123*, 7957–7958; b) J. J. E. Moreau, L. Vellutini, M. Wong Chi Man, C. Bied, *Chem. Eur. J.*, **2003**, *9*, 1594–1599; c) J. J. E. Moreau, B. P. Pichon, H. Pritzkow, M. Wong Chi Man, C. Bied, J. L. Bantignies, P. Dieudonné, J. L. Sauvajol, *Angew. Chem.* **2004**, *116*, 205–208; *Angew. Chem. Int. Ed.* **2004**, *43*, 203–206; d) O. J. Dautel, J. P. Lère-Porte, J. J. E. Moreau, M. Wong Chi Man, *Chem. Commun.* **2003**, 2662–2663; e) J. J. E. Moreau, B. P. Pichon, G. Arrachart, M. Wong Chi Man, C. Bied, *New J. Chem.*, **2005**, *29*, 653–658.
[7] a) M. Barboiu, G. Vaughan, A. van der Lee, *Org. Lett.* **2003**, *5*, 3073–3076; b) M. Barboiu, *J. Inclusion Phenom. Mol. Recognit. Chem.* **2004**, *49*, 133–137; c) M. Barboiu, S. Cerneaux, A. van der Lee, G. Vaughan, *J. Am. Chem. Soc.* **2004**, *126*, 3545–3550; d) A. Cazacu, C. Tong, A. van der Lee, T. M. Fyles, M. Barboiu, *J. Am. Chem. Soc.* **2006**, *128*, 9541–9548; e) M. Michau, M. Barboiu, R. Caraballo, C. Arnal-Hérault, A. van der Lee, unpublished results; f) C. Arnal-Hérault, A. Banu, M. Barboiu, M. Michau, A. van der Lee, *Angew. Chem.* **2007**, *119*, 4346–4350; *Angew. Chem. Int. Ed.*, **2007**, *46*, 4268–4272.
[8] a) J. L. Sessler, J. Jayawickramarajah, *Chem. Commun.* **2005**, 1939–1949; b) J. L. Sessler, C. M. Lawrence, J. Jayawickramarajah, *Chem. Soc. Rev.* **2007**, *36*, 314–325.
[9] a) J. T. Davis, *Angew. Chem.* **2004**, *116*, 684–716; *Angew. Chem. Int. Ed.* **2004**, *43*, 668–698; b) J. T. Davis, G. P. Spada, *Chem. Soc. Rev.* **2007**, *36*, 296–313.
[10] M. Numata, K. Sugiyasu, T. Hasegawa, S. Shinkai, S. *Angew. Chem.* **2004**, *116*, 3341–3345; *Angew. Chem. Int. Ed.* **2004**, *43*, 3279–3283.
[11] a) J. E. Freund, M. Edelwirth, P. Krobel, M. Heckl, *Phys. Rev. B* **1997**, *55*, 5394–5397; b) T. Uchihashi, T. Okada, Y. Sugawara, K. Yokoyama, S. Morita, *Phys. Rev. B* **1999**, *60*, 8309–8313; c) R. K. McMullan, P. Benci, B. M. Craven, *Acta Crystallogr. Sect. B* **1980**, *36*, 1424–1430; d) M. Mirzaei, N. L. Hadipour, *J. Phys. Chem. A* **2006**, *110*, 4833–4838; e) V. R. Pedireddi, A. Ranganathan, K. N. Ganesh, *Org. Lett.*, **2001**, *3*, 99–102.
[12] a) P. Piskorz, M. Wojcik, *J. Mol. Struct. THEOCHEM* **1995**, *332*, 217–223; b) M. Krzatochvil, O. Engkvist, J. Vacek, P. Jungwirth, P. Hobza, *Phys. Chem. Chem. Phys.* **2000**, *2*, 2419–2424.
[13] a) M. C. Etter, S. M. Reutzel, C. G. Choo, *J. Am. Chem. Soc.* **1993**, *115*, 4411–4412; b) R. K. Castellano, V. Gramlich, F. Diederich, *Chem. Eur. J.* **2002**, *8*, 118–129, and references therein; c) J. R. Quinn, S. C. Zimmerman, J. E. Del Bene, I. Shavitt, *J. Am. Chem. Soc.* **2007**, *129*, 934–941.
[14] Factors contributing to the preference for Hoogsteen geometry are the shorter C–H···O contacts, a favorable alignement of the dipoles, and a greater distance between secondary repulsive sites; see reference [13b,c] for details.

Received: May 16, 2007
Published online: July 17, 2007

